

First direct measurement of the $^{11}\text{C}(\alpha, p)^{14}\text{N}$ stellar reaction by an extended thick-target method

S. Hayakawa,^{1,*} S. Kubono,^{1,2,3} D. Kahl,^{1,†} H. Yamaguchi,¹ D. N. Binh,⁴ T. Hashimoto,⁵
Y. Wakabayashi,² J. J. He,³ N. Iwasa,⁶ S. Kato,⁷ T. Komatsubara,² Y. K. Kwon,⁵ and T. Teranishi⁸

¹*Center for Nuclear Study, the University of Tokyo,*

RIKEN campus, 2-1 Hirosawa, Wako, Saitama 351-0198, Japan

²*RIKEN Nishina Center, 2-1 Hirosawa, Wako, Saitama 351-0198, Japan*

³*Institute of Modern Physics, Chinese Academy of Science,*

Nanchang Road 509, Lanzhou 730000, People's Republic of China

⁴*Institute of Physics, Vietnamese Academy for Science and Technology, 10 Daotan, Thule, Badinh, Hanoi, Vietnam*

⁵*Rare Isotope Science Project, Institute for Basic Science, Yuseong-gu Daejeon 305-811, Republic of Korea*

⁶*Department of Physics, Tohoku University, Aoba, Sendai, Miyagi 980-8578, Japan*

⁷*Department of Physics, Yamagata University, 1-4-12 Kojirakawa-machi, Yamagata 990-8560, Japan*

⁸*Department of Physics, Kyushu University, 744 Motoooka, Nishi-ku, Fukuoka 819-0395, Japan*

(Dated: September 27, 2016)

The $^{11}\text{C}(\alpha, p)^{14}\text{N}$ reaction is an important α -induced reaction competing with β -limited hydrogen-burning processes in high-temperature explosive stars. We directly measured its reaction cross sections both for the ground-state transition (α, p_0) and the excited-state transitions (α, p_1) and (α, p_2) at relevant stellar energies 1.3–4.5 MeV by an extended thick-target method featuring time of flight for the first time. We revised the reaction rate by numerical integration including the (α, p_1) and (α, p_2) contributions and also low-lying resonances of (α, p_0) using both the present and the previous experimental data which were totally neglected in the previous compilation works. The present total reaction rate lies between the previous (α, p_0) rate and the total rate of the Hauser-Feshbach statistical model calculation, which is consistent with the relevant explosive hydrogen-burning scenarios such as the νp -process.

PACS numbers: 29.30.Ep, 26.30.-k, 24.30.-v, 25.55.-e

I. INTRODUCTION

Hydrogen burning at high temperatures of the order of $T_9 \sim 0.1\text{--}1$ (T_9 represents 1 GK) is of great importance in terms of production of heavy elements beyond iron and energy generation in various high-temperature and explosive astrophysical sites, such as supermassive metal-poor stars, type-I x-ray bursts, and core-collapse supernovae. The nucleosynthesis paths and the timescale of the rp -process in such stellar environments depend on the simultaneously occurring αp -process [1]. This process breaks out from the hot CNO cycle and bypasses slower β -decays by sequences of (α, p) reactions and proton captures up to mass number $A \sim 40$, drastically depending on temperature. In type-I x-ray bursts, which are the most frequent nuclear explosion in the universe [2], the αp -process may determine the time evolution of energy release which varies by 2–3 orders of magnitude in about 1 second, and thus several key (α, p) reactions, *e.g.* $^{14}\text{O}(\alpha, p)^{17}\text{F}$ and $^{18}\text{Ne}(\alpha, p)^{21}\text{Na}$, have been investigated [3]. Some studies for metal-poor stars [4] and the νp -process [5] suggest that several α -induced reaction sequences, such as $^7\text{Be}(\alpha, \gamma)^{11}\text{C}(\alpha, p)^{14}\text{N}$ and $^7\text{Be}(\alpha, p)^{10}\text{B}(\alpha, p)^{13}\text{C}$, also

may appear significant in $T_9 = 1.5\text{--}3$. These sequences are shown to bridge the mass gap at $A = 8$ comparably to the triple- α process, which may even affect the abundances of p -nuclei around $A = 90$ [5].

The current problem in nucleosynthesis is that most of the relevant (α, p) reaction rates have been estimated only through studies on resonances, time-reversal reactions, or other indirect methods, with only a few direct measurements [6–9]. These direct measurements provided limited results due to experimental difficulties, such as detection efficiency, production of radioactive ion beams, determination of reaction points in the ^4He gas target, identification of the final excited states, etc. Recently, some research projects for direct measurement of (α, p) reactions of astrophysical interest are ongoing using an ambitious detection system such as HELIOS (Helical Orbit Spectrometer [10, 11]), which has been used for (d, p) reaction measurements, yet under commissioning for (α, p) reaction measurements. Besides these works, we have successfully performed a direct measurement of the $^{11}\text{C}(\alpha, p)^{14}\text{N}$ reaction for the first time by a simple experimental configuration, leading one of the most comprehensive results among the above crucial nucleosynthesis paths.

The $^{11}\text{C}(\alpha, p)^{14}\text{N}$ reaction rates currently available are reported in compilations by Caughlan and Fowler [12] (hereafter “CF88”), and NACRE collaboration [13]. Both of them are based on studies of the time-reversal reaction $^{14}\text{N}(p, \alpha)^{11}\text{C}$ by the activation method [14–19],

* hayakawa@cns.s.u-tokyo.ac.jp

† Present address: School of Physics and Astronomy, the University of Edinburgh, James Clerk Maxwell Building, Peter Guthrie Tait Road, Edinburgh, EH9 3FD, UK

which thus provide information only on the transition to the ground state of ^{14}N (hereafter “ (α, p_0) ”), but not to the excited states (hereafter “ (α, p_1) ”, “ (α, p_2) ”, etc.). Indeed, in nuclear astrophysics, transitions to excited states are rarely investigated experimentally in spite of their importance. In the CF88 compilation, the astrophysical S -factor of this reaction as well as that of the time-reversal reaction were adopted from the lowest-energy study by Ingalls *et al.* [18] which approximated the cross section over several resonances by a smooth function. The NACRE compilation derived the S -factor of the time-reversal reaction from 6 data sets [14–19] with improvement at higher energies, but it obviously underestimated the lowest energy part which is important for the reaction rate near T_9 temperatures. An alternative compilation work on the $^{14}\text{N}(p, \alpha)^{11}\text{C}$ reaction by Takács *et al.* [20] has applied the Padé approximation to the excitation functions of 13 data sets up to $E_{\text{c.m.}} \sim 25$ MeV in the $^{11}\text{C} + \alpha$ center-of-mass system reproducing resonances more properly, but the resonances below $E_{\text{c.m.}} = 1.5$ MeV were again just smoothed out. A direct measurement is able to address the above omissions in the reaction rate evaluations, and also enables us to observe such excited-state transitions and also has an advantage to validate the cross sections measured by the activation method.

II. EXPERIMENTAL METHOD AND DATA ANALYSIS

The experiment was performed in inverse kinematics using the unstable nuclide ^{11}C as the projectile covering a center-of-mass energy range 0–4.5 MeV based on the thick target method [21]. The ^{11}C beams were produced by the in-flight technique with CRIB (Center for Nuclear Study Radioactive Ion Beam separator [22]). A $^{11}\text{B}^{3+}$ primary beam at 4.6 MeV/nucleon with a typical intensity of 1 μA was provided by the RIKEN AVF cyclotron, and bombarded the cryogenic hydrogen gas target [23] with a typical thickness of 1.7 mg/cm^2 , confined by 2.5- μm -thick Havar foils at beam entrance and exit. The secondary ^{11}C ions produced via the $^1\text{H}(^{11}\text{B}, ^{11}\text{C})n$ reaction were purified by the double achromatic system and the following Wien filter of CRIB.

The experimental setup at the final focal plane, illustrated in Fig. 1, consisted of two beam-line monitors, a ^4He gas target, and three sets of ΔE -E position-sensitive silicon detector telescopes. A Parallel Plate Avalanche Counter (PPAC) [24] was used for the first beam-line monitor, and another PPAC and a MicroChannel Plate detector (MCP) [25] were switchable for the second monitor; the employed experimental setup allowed us to alternate between two different on-target energies by the different thicknesses of the second beam-line monitors, thus scanning a wide excitation-energy range in two measurements without altering the CRIB optical condition. This setup was also helpful to confirm self-consistency of

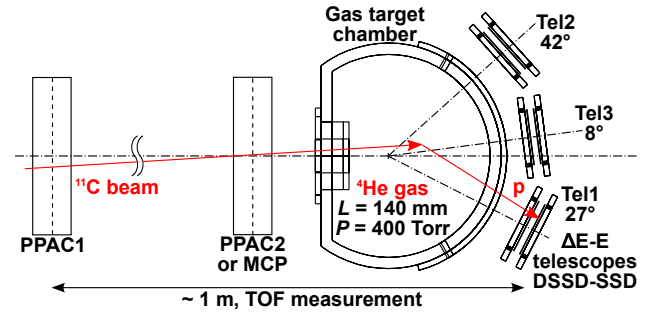


FIG. 1. (Color online) Plane view of the experimental setup.

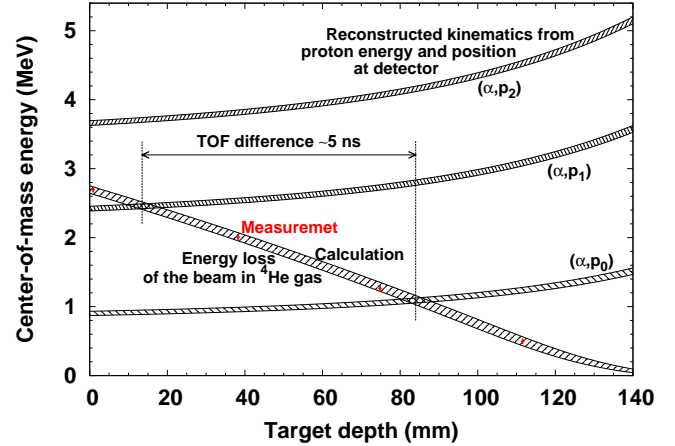


FIG. 2. (Color online) Example of the center-of-mass energies as functions of the target depth. The decreasing function is determined from the energy loss calculation with the incident beam energy of 10.12 ± 0.46 MeV, which is consistent with the actual measurement shown as red crosses. The increasing functions are reconstructed by kinematic calculations and energy loss corrections of a detected proton for (α, p_0) , (α, p_1) and (α, p_2) with a given kinetic energy of 5 MeV and a scattering angle of 40° . The vertices of these functions represent the possible reaction energy and position.

our measurement by checking the data in the overlapping energy region of the lower- and the higher-energy run, as mentioned later. These two monitors tracked each beam particle event-by-event, and the first monitor also acted as the time reference of the measurement. The data acquisition was triggered by the sum of the down-scaled signal of the first PPAC and the coincident signal of the first PPAC with the silicon detectors, which thus canceled out the PPAC efficiency for the absolute cross section determination. The two resulting beam energies were directly measured with a silicon detector at the target position, to be 10.12 ± 0.46 MeV and 16.86 ± 0.36 MeV in full width at half maximum, covering center-of-mass energy ranges 0–2.7 MeV and 2.3–4.5 MeV, respectively. The secondary-beam ions were identified event by event from the time of flight (TOF) information between the two beam-line monitors and the TOF with respect to the cyclotron radio-frequency signal, thus the beam con-

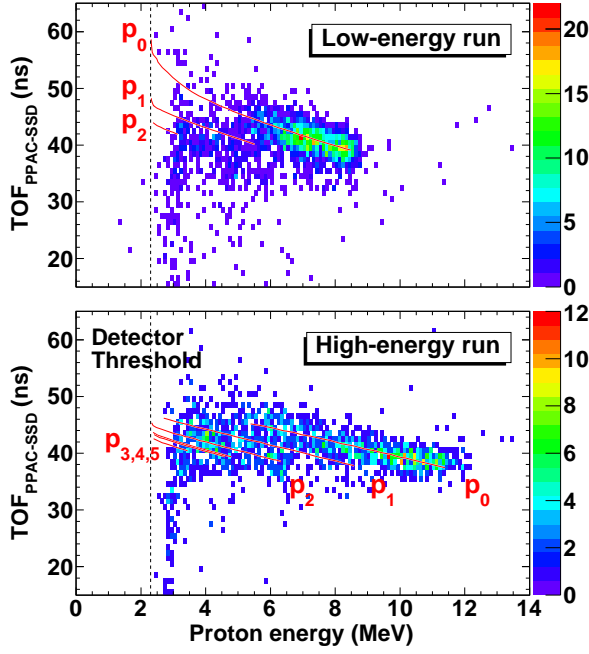


FIG. 3. (Color online) TOF from the first PPAC to the SSD versus energy of protons detected in Tel1 of the lower-energy run (upper) and the higher-energy run (lower) with calculated lines for allowed excited-state transitions.

taminants were easily distinguished in the analysis. The $^{11}\text{C}^{6+}$ purity was determined to be higher than 97%, and the rest was mostly $^{11}\text{B}^{5+}$ and trace amounts of $^{11}\text{C}^{5+}$. The ^{11}C beam spot was well focused on the target window with a diameter of 30 mm so that 78% of the ^{11}C beam particles eventually entered the target chamber, and the on-target average intensities of the lower- and the higher-energy ^{11}C beams were 3.1×10^5 pps and 1.0×10^5 pps, respectively.

The ^4He gas target was sealed with 2.5- μm -thick Havar foil at the entrance window, and 25- μm -thick Mylar foil at the exit window which is in a cylindrical shape and has a sufficiently large area for the full detection acceptance. The energy straggling of the ejected proton through this exit window is estimated at only 20 keV at most, which is negligible.

The silicon telescopes were mounted at three different laboratory angles, 27° , 42° and 8° (labeled as “Tel1”, “Tel2” and “Tel3”, respectively), facing the geometrical center of the arc of the exit window of the gas target. The active area of each silicon detector was $50 \times 50 \text{ mm}^2$, and the ΔE layers were double-sided stripped silicon detectors (DSSDs) with 16 strips in two orthogonal dimensions with typical thicknesses of 30-60 μm , and the E layers were single-pad (SSDs) with typical thicknesses of 1.5 mm in which the protons were fully stopped. The observed particles with the ΔE -E telescopes are mostly identified as protons and alphas with sufficient resolution, together with a few deuterons and ^3He ions.

The present experimental setup is remarkable in terms of the use of an extended gas target with a length of

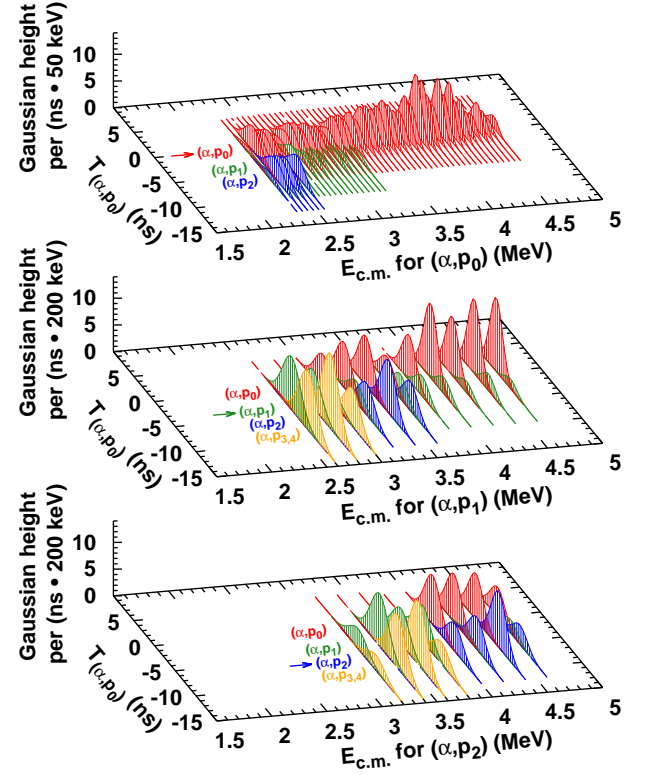


FIG. 4. (Color online) Gaussian functions fitted to the data of Tel1 with the higher-energy beam at each calculated locus within each energy bin. The energy bin sizes are 50 keV for (α, p_0) and 200 keV for (α, p_1) and (α, p_2) . The extracted excited state loci are indicated by arrows. The same treatment has been also applied to the other telescopes, and the lower-energy data.

140 mm along the beam axis at a pressure of 400 Torr, which enables separation of each transition to the ^{14}N excited state ($E_x = 2.313 \text{ MeV}$, 3.948 MeV , etc.) to be observed in different TOF between the first PPAC and the SSDs. A similar idea was previously proposed in Ref. [26] and two experiments at CRIB [27, 28], but none of them actually deduced cross sections for excited-state transitions separately. A more detailed explanation of this technique was given by Ref. [29] for separation of proton elastic and inelastic scatterings with a ^7Be beam. However, again they did not demonstrate the TOF separation of the actual data due to insufficient time difference for the first excitation energy of ^7Be 0.43 MeV, but showed the separation in the energy correlation between the light and the heavy recoil particles with the hybrid thick/thin target method. Thus here we have for the first time made the full proof of principle for the (α, p) reaction measurement with the TOF technique in a comprehensive way.

Figure 2 illustrates how to determine the center-of-mass energies as well as the target position for a reaction event, under a given condition with a proton kinetic energy of 5 MeV, a scattering angle of 40° , and the lower beam energy. For the basis of this method, we di-

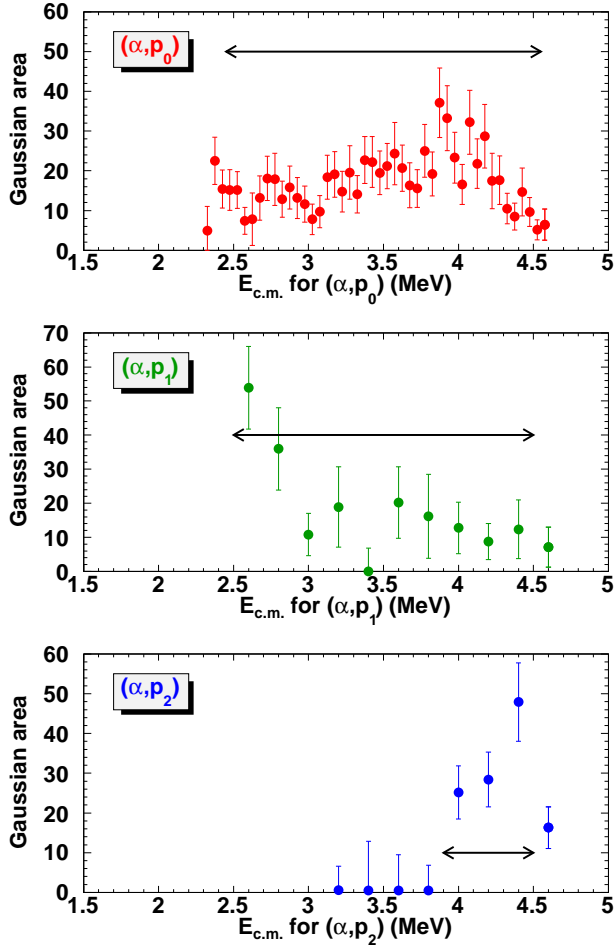


FIG. 5. (Color online) Numbers of events of (α, p_0) , (α, p_1) and (α, p_2) . Each value represents the area of the corresponding Gaussian function extracted from those drawn in Fig. 4 (Tel1, higher-energy run). The arrows indicate the energy ranges selecting only the reliable data. The same treatment has been also applied to the other telescopes, and the lower-energy data.

rectly measured the energy loss (red cross) and straggling (vertical error bar) of the ^{11}C beam particles at several ^4He gas target depths with a silicon detector inside the gas, and confirmed consistency with energy loss calculation [30] shown as a decreasing function. On the other hand, the increasing functions represent possible kinematic conditions of different excited-state transitions for a detected proton taking into account energy loss in the target gas with the above given energy and angle. The widths of these functions represent the systematic uncertainties. Therefore one can determine the reaction energy and position simultaneously as the vertex of these functions. The typical distance between reaction positions of (α, p_0) and (α, p_1) calculated by this method is about 70 mm, where the equivalent TOF difference becomes about 5 ns. This TOF difference enables one to identify which excited state in ^{14}N the reaction reaches event by event. With a Monte Carlo simulation, we estimated

the accuracy of the center-of-mass energy 45–65 keV depending on the intrinsic energy resolution of each silicon telescope and the reaction angle; we found that the typical determination accuracy of reaction position is about 5 mm, implying that the uncertainty in the solid angle is eventually smaller than the statistical error we observed.

Figure 3 shows the relation between the TOF from the first PPAC to the SSD against the energy of protons detected in Tel1 of the lower- and the higher-energy runs. The calculated TOF values are shown as solid lines for several allowed excited-state transitions, of which the properties such as the onset of energy and the gradient nicely agree with the measured distributions in the plot. The energy dependence of the time resolution of the SSDs was apparently independent from the choice of the beam condition, thus it was estimated from the time broadening of (α, p_0) -only loci of the lower- and the higher-energy ^{11}C beam data and the ^{11}B primary beam data. The time broadening gradually increases from 1 ns to 3 ns as the proton energy decreases from 12 MeV to 4 MeV, and almost diverges very close to the energy threshold limited by the ΔE thickness, appearing in Fig. 3. Such a time broadening can be regarded as the intrinsic SSD resolution as the effects of the proton scattering angle or the beam energy broadening are expected to be sufficiently small. Although the separation of different excited-state loci was not perfect due to the time broadening, we successfully extracted their mixing ratios by fitting Gaussian functions to the time spectra within limited energy bins as described below.

Figure 4 and 5 demonstrate the procedure to determine the number of events N for each excited-state transition from the same data (Tel1, higher-energy run) as Fig. 3. We fitted those data projected to the time axis by Gaussian functions at each calculated peak within each energy bin. The result of the fitting is shown in Fig. 4. Note that the origin of the time axis of Fig. 4 is realigned to the calculated (α, p_0) locus, which leads better separation between different loci within a finite size of an energy bin. The energy axes in Fig. 4 and 5 are converted to the center-of-mass energies $E_{\text{c.m.}}$ reconstructed with the Q -values for (α, p_0) (top panel, $Q_0 = 2.923$ MeV), (α, p_1) (middle panel, $Q_1 = 0.610$ MeV) and (α, p_2) (bottom panel, $Q_2 = -1.030$ MeV), respectively. The $E_{\text{c.m.}}$ bin sizes were 50 keV for (α, p_0) , and 200 keV for (α, p_1) and (α, p_2) . Each excited-state locus in Fig. 4 is labeled as (α, p_0) etc., and the arrows indicate which locus is extracted. Figure 5 shows the extracted numbers of events of (α, p_0) , (α, p_1) and (α, p_2) as the area of the corresponding Gaussian function N defined by

$$N = \sqrt{2\pi} \frac{H\sigma}{\Delta t_{\text{bin}}}, \quad (1)$$

where H and σ are the height and the width of the Gaussian function respectively, and $\Delta t_{\text{bin}} = 1$ ns is the bin size of the normalized time $T_{(\alpha, p_0)}$. Thus the error of the counts ΔN , namely, that of the area of the Gaussian

function can be defined as

$$\Delta N = N \sqrt{\left(\frac{\Delta H}{H}\right)^2 + \left(\frac{\Delta \sigma}{\sigma}\right)^2}, \quad (2)$$

where Δh and $\Delta \sigma$ are the error of the fitted parameters. The arrows in Fig. 5 indicate the energy ranges selecting only the reliable data, eliminating the data at the ends of the energy ranges, and the (α, p_2) data below the onset energy of (α, p_3) as they overlap considerably. We repeated the same procedure for the data of the other telescopes, and also for the lower-energy run.

We also performed a measurement with the same setup but the gas target filled with argon gas of an equivalent thickness in order to subtract background protons which reached only the most forward telescope (Tel3) passing through the gas target windows from upstream in coincidence with the beam particles triggering. Such protons were also identified by the TOF-versus-energy information in a larger time range and mostly separated from the (α, p) reaction events. The only influential case was protons from the Mylar foil of the second PPAC produced by elastic scattering of beam particles, which partially overlapped with the (α, p_1) and the (α, p_2) data of comparable intensity. We only eliminated these data, otherwise the angular distribution of the background-subtracted data of Tel3 were basically consistent with the corresponding data of Tel1 and Tel2 within the errors, which were taken into account to the angle-averaged cross sections as discussed later.

III. ASTROPHYSICAL S -FACTORS

The present data appear to be nearly isotropic, because 94% of the data points are located within a factor of 2 or less from the weighted mean value of the angular distribution spread at each energy. This is shown up in Fig. 6 as the ratio of the observed differential cross section to that of the weighted average at each energy versus the center-of-mass angle. The angular distributions of the lower- and the higher-energy runs in their overlapping range from 2.30 MeV to 2.75 MeV were also in agreement within their errors, which confirms the self-consistency of our measurements.

In Fig. 7, the newly obtained astrophysical S -factors of both the lower-energy run and the higher-energy run for (α, p_0) , (α, p_1) and (α, p_2) are plotted as red solid circles with error bars. The crosses with error bars are from the time-reversal reaction data [18] with the detailed balance theorem. The Gamow windows of $T_9 = 1.5$ and 3 are indicated with arrows in the bottom panel. For comparison, the Hauser-Feshbach model calculations for each transition by the code NON-SMOKER^{WEB} [31, 32] are shown as the dashed curve in the respective panels, and the (α, p_0) S -factors of CF88 [12] (dotted curve) and that of Takács *et al.* [20] (dashed-dotted curve) are shown together in the top panel.

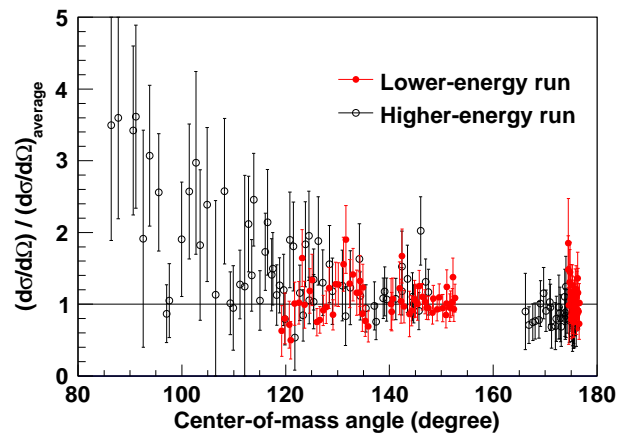


FIG. 6. (Color online) Ratio of the observed differential cross section to that of the weighted average at each energy versus the center-of-mass angle. The red solid circles are of the lower-energy run and the black open circles are of the higher-energy run.

The (α, p_0) S -factor by the Hauser-Feshbach calculation roughly agrees with the present experimental data within a factor of 2 over a several MeV range, but obviously overestimates the rate at the lowest energies. One can see that the present (α, p_0) data are mostly consistent with the previous data by Ref. [18] and [20] over most of the energy range except near the lower energy limit of the measurement around 1.3 MeV. The peak position in the present work near the known resonance at 1.349 MeV looks shifted to a slightly lower energy. At the lowest energies below $E_{c.m.} = 1.3$ MeV, the yield of the (α, p_0) events rapidly dropped, and not all of the three telescopes counted reliable (α, p_0) events. Thus the angle-integrated cross section of these data are lacking over some angular ranges, and so we adopted the data only above that energy for the reaction rate calculation.

The 8 arrows in the top panel indicate the positions of the known low-lying resonances with significant total widths, corresponding well to the peaks appearing in the experimental data. For known excited levels [33] in the corresponding energy region, most resonance energies and total widths have been well determined via proton elastic and inelastic scattering on ^{14}N , and some spins, parities and orbital angular momenta were assigned by R -matrix analysis [34, 35], but no α partial widths were known. Here we do not demonstrate R -matrix analysis on these data, because we have only limited statistics for each resonances, the resonance widths are comparable to the energy resolution, and the most resonances overlap each other, which would unlikely lead any new information or constraints beyond what was determined in the previous works. We also observed the excitation function of the α elastic scattering down to $E_{c.m.} \sim 2$ MeV with some resonant structure at the most forward angles even below the Coulomb barrier of 3.5 MeV. However, no useful information could be extracted in the lower energy range to which the reaction rate below $T_9 = 3$ is

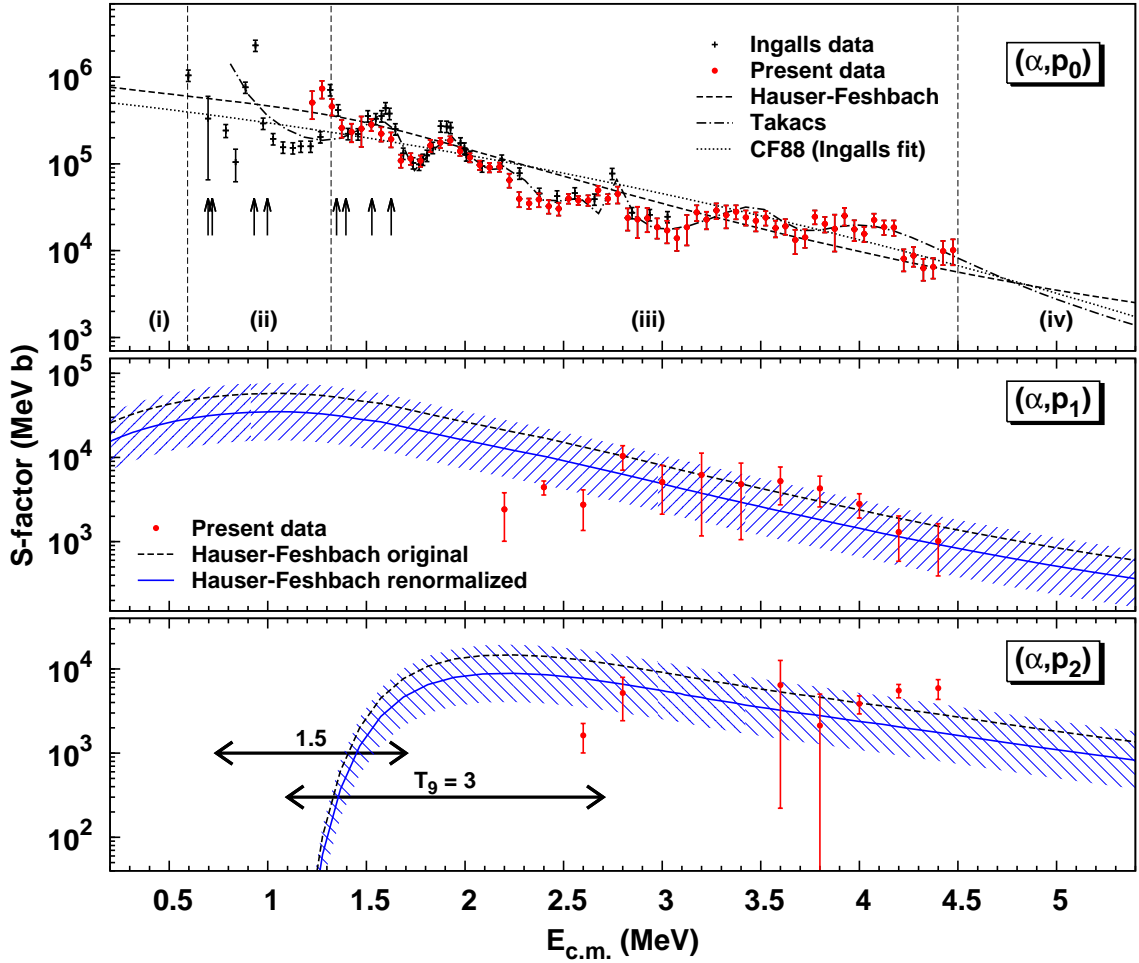


FIG. 7. (Color online) S -factors for $^{11}\text{C}(\alpha, p_0)^{14}\text{N}$ (top), $^{11}\text{C}(\alpha, p_1)^{14}\text{N}^*$ (middle) and $^{11}\text{C}(\alpha, p_2)^{14}\text{N}^*$ (bottom). The present data of both the lower-energy run and the higher-energy run are shown as red solid circles with error bars. The original Hauser-Feshbach calculations for each excited-state transition are shown as dashed curve, respectively. In the (α, p_0) panel, the data of Ingalls *et al.* [18] (cross with error bars), and compilation curves of CF88 [12] and Takács *et al.* [20] are also shown for comparison, and the arrows indicates the most significant 8 energies of the known resonances below 1.7 MeV. For (α, p_1) and (α, p_2) , the renormalized Hauser-Feshbach curves (solid curve) to the present data with their errors (hatch) are also shown.

sensitive. Thus we neglected to pursue further analysis of these data in this paper.

The present (α, p_1) and the (α, p_2) cross sections come out about one order of magnitude lower than the (α, p_0) one, and those of the Hauser-Feshbach calculation appear to be larger than the present experimental data. For the reaction rate calculation, we extrapolated those S -factors toward the full energy range using the shape of the Hauser-Feshbach calculations renormalizing to the present data by the logarithmic least-squares method. Note that the utilization of the statistical model is not to justify its applicability to such a light nuclear system, but rather to reveal difference of its absolute value. The renormalized Hauser-Feshbach curves are shown in addition to the original ones in the middle and the bottom panels of Fig. 7. The normalization factors for (α, p_1) and (α, p_2) are 0.61 and 0.69, and their logarithmic standard deviations are 2.2 and 2.6, respectively, as drawn

with hatched areas.

IV. REACTION RATES

To derive the total reaction rate of $^{11}\text{C}(\alpha, p)^{14}\text{N}$, we adopted new S -factors based on all presently available data as follows. The (α, p_0) data were selected from each energy section defined as (i)–(iv) by vertical dashed lines in Fig. 7; (i) the CF88 smooth curve, (ii) the data points of the time-reversal reaction [18], (iii) the present data points, (iv) the compilation of Ref. [20] up to 25 MeV. For (α, p_1) and (α, p_2) , we adopted the present data points for the measured energy regions, otherwise the renormalized Hauser-Feshbach curves as extrapolation. We performed numerical integration of those S -factors based on Simpson's rule in energy ranges where the integrated values converged well. For the integration, the values at en-

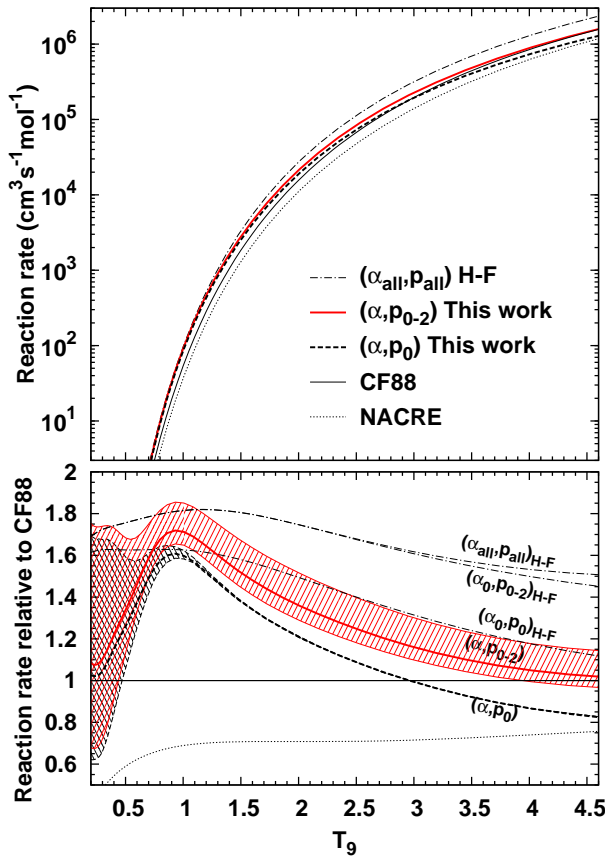


FIG. 8. (Color online) Absolute $^{11}\text{C}(\alpha, p)^{14}\text{N}$ reaction rates of the present data and the currently available ones (upper) and their ratios to the CF88 one (lower). The uncertainties of the present (α, p_0) rate and total rate are drawn as hatches attached in the bottom panel.

ergies in between data points were linearly interpolated from the neighboring values.

Figure 8 shows the absolute reaction rates (upper) and the reaction rates relative to the CF88 rate (lower) of the present data and several previously reported ones. The hatched regions in the lower panel indicate the errors of the present rates. The error of (α, p_0) arises only from an uncertainty of a factor of 1.65 in the energy section (i) estimated as the logarithmic standard deviation of the present data against the CF88 curve, while those of (α, p_1) and (α, p_2) from the uncertainties of the renormalized Hauser-Feshbach functions. In the νp -process temperature range ($T_9 = 1.5\text{--}3$) [5], the present (α, p_0) reaction rate is enhanced from the CF88 rate by about 40% at most, mainly due to the resonances around 0.9 MeV and 1.35 MeV which were not taken into account at all in neither CF88, NACRE nor Ref. [20]. The contribution from the (α, p_1) and (α, p_2) reaction rate to the to-

tal reaction rate is about 20% of the (α, p_0) at most, and the error of the total reaction rate results in about 15%. The Hauser-Feshbach rate for (α, p_0) overestimates at low temperatures and approaches to the experimental rates as the temperature increases, as expected from the behavior of its S -factor in Fig. 7. The Hauser-Feshbach model calculation for the excited states shows an insignificant difference between the (α, p_{0-2}) rates and the total rate $(\alpha_{\text{all}}, p_{\text{all}})$, which suggests the present measurement up to (α, p_2) is sufficient.

As for the astrophysical implications of the present work, it turns out that the enhancement of the $^{11}\text{C}(\alpha, p)^{14}\text{N}$ reaction rate by less than a factor of two would not be a big impact to change the relevant nuclear-burning scenarios; by the present reaction rate, the deviation of the branching condition between the $^{11}\text{C}(\alpha, p)^{14}\text{N}$ reaction and the ^{11}C β -decay from the previous condition [4] is negligible, as the neighbor branching conditions of other reactions are located so far from that of this reaction by many order of magnitude in the density-energy dependency investigated for metal-poor stars. Therefore we conclude that the present result could also support the validity of this reaction as a possible path which breaks out from the pp -chain region to the CNO-cycle region in the νp -process [5].

V. SUMMARY

We have performed a direct measurement of the $^{11}\text{C}(\alpha, p)^{14}\text{N}$ reaction cross section at stellar energies of 1.3–4.5 MeV by the extended thick-target method, which enabled separation of both the (α, p_0) , (α, p_1) and (α, p_2) transitions in time of flight. The present measurement provided one of the most comprehensive results among relevant stellar (α, p) reactions under explosive burning conditions. The new total reaction rate lies between the previous (α, p_0) rate and the total Hauser-Feshbach rate, which still supports the validity of relevant explosive hydrogen-burning process scenarios such as the νp -process that it proceeds via the $^{11}\text{C}(\alpha, p)^{14}\text{N}$ reaction in addition to the triple- α process. We expect that the present extended thick-target method with the TOF technique is widely applicable to other α - or even proton-induced reaction or scattering measurements.

ACKNOWLEDGMENTS

We thank the accelerator staff at RIKEN and CNS, Prof. T. Rauscher for his help with the NON-SMOKER calculations, and Dr. S. Wanajo for productive discussions on the νp -process. This work was partly supported by JSPS KAKENHI (Grant No. 25800125 and 21340053).

[1] R. K. Wallace and S. E. Woosley, *Astrophys. J. Suppl. Ser.* **45**, 389 (1981).

[2] J. L. Fisker, H. Schatz, and F.-K. Thielemann, *Astrophys. J. Suppl. Ser.* **174**, 261 (2008).

- [3] P. Mohr and A. Matic, *Phys. Rev. C* **87**, 035801 (2013).
- [4] M. Wiescher, J. Gorres, S. Graff, L. Buchmann, and F.-K. Thielemann, *Astrophys. J.* **343**, 352 (1989).
- [5] S. Wanajo, H. T. Janka, and S. Kubono, *Astrophys. J.* **729**, 46 (2011).
- [6] A. A. Sonzogni, K. E. Rehm, I. Ahmad, F. Borasi, D. L. Bowers, F. Brumwell, J. Caggiano, C. N. Davids, J. P. Greene, B. Harss, A. Heinz, D. Henderson, R. V. F. Janssens, C. L. Jiang, G. McMichael, J. Nolen, R. C. Pardo, M. Paul, J. P. Schiffer, R. E. Segel, D. Seweryniak, R. H. Siemssen, J. W. Truran, J. Uusitalo, I. Wiedenhöver, and B. Zabransky, *Phys. Rev. Lett.* **84**, 1651 (2000).
- [7] W. Bradfield-Smith, T. Davinson, A. Di Pietro, A. M. Laird, A. N. Ostrowski, A. C. Shotton, P. J. Woods, S. Cherubini, W. Galster, J. S. Graulich, P. Leleux, L. Michel, A. Ninane, J. Vervier, J. Görres, M. Wiescher, J. Rahighi, and J. Hinfefeld, *Phys. Rev. C* **59**, 3402 (1999).
- [8] D. Groombridge, A. C. Shotton, W. Bradfield-Smith, S. Cherubini, T. Davinson, A. Di Pietro, J. Görres, J. S. Graulich, A. M. Laird, P. Leleux, A. Musumarra, A. Ninane, A. N. Ostrowski, J. Rahighi, H. Schatz, M. Wiescher, and P. J. Woods, *Phys. Rev. C* **66**, 055802 (2002).
- [9] M. Notani, S. Kubono, T. Teranishi, Y. Yanagisawa, S. Michimasa, K. Ue, J. J. He, H. Iwasaki, H. Baba, M. Tamaki, T. Minemura, S. Shimoura, N. Hokoïwa, Y. Wakabayashi, T. Sasaki, T. Fukuchi, A. Odahara, Y. Gono, Z. Fülöp, E. K. Lee, K. I. Hahn, J. Y. Moon, C. C. Yun, J. H. Lee, C. S. Lee, and S. Kato, *Nucl. Phys. A* **746**, 113c (2004).
- [10] A. H. Wuosmaa, J. P. Schiffer, B. B. Back, C. J. Lister, and K. E. Rehm, *Nucl. Instrum. Methods A* **580**, 1290 (2007).
- [11] J. C. Lighthall, B. B. Back, S. I. Baker, S. J. Freeman, H. Y. Lee, B. P. Kay, S. T. Marley, K. E. Rehm, J. E. Rohrer, J. P. Schiffer, D. V. Shetty, A. W. Vann, J. R. Winkelbauer, and A. H. Wuosmaa, *Nucl. Instrum. Methods A* **622**, 97 (2010).
- [12] G. R. Caughlan and W. A. Fowler, *At. Data Nucl. Data Tables* **40**, 283 (1988).
- [13] C. Angulo, M. Arnould, M. Rayet, P. Descouvemont, D. Baye, C. Leclercq-Willain, A. Coc, S. Barhoumi, P. Aguer, C. Rolfs, R. Kunz, J. W. Hammer, A. Mayer, T. Paradellis, S. Kossionides, C. Chronidou, K. Spyrou, S. Degl'Innocenti, G. Fiorentini, B. Ricci, S. Zavatarelli, C. Providencia, H. Wolters, J. Soares, C. Grama, J. Rahighi, A. Shotton, and M. L. Racht, *Nucl. Phys. A* **656**, 3 (1999).
- [14] P. Shrivastava, F. Boreli, and B. Kinsey, *Phys. Rev.* **169**, 842 (1968).
- [15] W. W. Jacobs, D. Bodansky, D. Chamberlin, and D. L. Oberg, *Phys. Rev. C* **9**, 2134 (1974).
- [16] V. R. Casella, D. R. Christman, T. Ido, and A. P. Wolf, *Radiochimica Acta* **25**, 17 (1978).
- [17] M. Epherre and C. Seide, *Phys. Rev. C* **3**, 2167 (1971).
- [18] P. D. Ingalls, J. S. Schweitzer, B. D. Anderson, and M. Rios, *Phys. Rev. C* **13**, 524 (1976).
- [19] G. T. Bida, T. J. Ruth, and A. P. Wolf, *Radiochimica Acta* **27**, 181 (1980).
- [20] S. Takács, F. Tárkányi, A. Hermanne, and R. P. de Corcuera, *Nucl. Instrum. Methods B* **211**, 169 (2003).
- [21] K. P. Artemov, O. P. Belyanin, A. L. Vetoshkin, R. Wolski, M. S. Golovkov, V. Z. Goldberg, M. Madeja, V. V. Pankratov, I. N. Serikov, V. A. Timofeev, V. N. Shadrin, and J. Szmider, *Sov. J. Nucl. Phys.* **52**, 408 (1990).
- [22] Y. Yanagisawa, S. Kubono, T. Teranishi, K. Ue, S. Michimasa, M. Notani, J. J. He, Y. Ohshiro, S. Shimoura, S. Watanabe, N. Yamazaki, H. Iwasaki, S. Kato, T. Kishida, T. Morikawa, and Y. Mizoi, *Nucl. Instrum. Methods A* **539**, 74 (2005).
- [23] H. Yamaguchi, Y. Wakabayashi, G. Amadio, S. Hayakawa, H. Fujikawa, S. Kubono, J. J. He, A. Kim, and D. N. Binh, *Nucl. Instrum. Methods A* **589**, 150 (2008).
- [24] H. Kumagai, A. Ozawa, N. Fukuda, K. Sümmerer, and I. Tanihata, *Nucl. Instrum. Methods A* **470**, 562 (2001).
- [25] S. Hayakawa, Master's thesis, Department of Physics, the University of Tokyo (2008).
- [26] C. Fu, V. Z. Goldberg, A. M. Mukhamedzhanov, G. G. Chubarian, G. V. Rogachev, B. Skorodumov, M. McCleskey, Y. Zhai, T. Al-Abdullah, G. Tabacaru, L. Trache, and R. E. Tribble, *Phys. Rev. C* **76**, 021603 (2007).
- [27] H. S. Jung, C. S. Lee, Y. K. Kwon, J. Y. Moon, J. H. Lee, C. C. Yun, S. Kubono, H. Yamaguchi, T. Hashimoto, D. Kahl, S. Hayakawa, S. Choi, M. J. Kim, Y. H. Kim, Y. K. Kim, J. S. Park, E. J. Kim, C.-B. Moon, T. Teranishi, Y. Wakabayashi, N. Iwasa, T. Yamada, Y. Togano, S. Kato, S. Cherubini, and G. G. Rapisarda, *Phys. Rev. C* **85**, 045802 (2012).
- [28] A. Kim, N. H. Lee, M. H. Han, J. S. Yoo, K. I. Hahn, H. Yamaguchi, D. N. Binh, T. Hashimoto, S. Hayakawa, D. Kahl, T. Kawabata, Y. Kurihara, Y. Wakabayashi, S. Kubono, S. Choi, Y. K. Kwon, J. Y. Moon, H. S. Jung, C. S. Lee, T. Teranishi, S. Kato, T. Komatsubara, B. Guo, W. P. Liu, B. Wang, and Y. Wang, *Phys. Rev. C* **92**, 035801 (2015).
- [29] G. V. Rogachev, E. D. Johnson, J. Mitchell, V. Z. Goldberg, K. W. Kemper, and I. Wiedenhöver, *AIP Conf. Proc.* **1213**, 137 (2010).
- [30] J. F. Ziegler, M. D. Ziegler, and J. P. Biersack, *Nucl. Instrum. Methods B* **268**, 1818 (2010).
- [31] P. Descouvemont and T. Rauscher, *Nucl. Phys. A* **777**, 137 (2006).
- [32] T. Rauscher (private communication).
- [33] F. Ajzenberg-Selove, *Nucl. Phys. A* **523**, 1 (1991).
- [34] M. West, C. Jones, J. Bair, and H. Willard, *Phys. Rev.* **179**, 1047 (1969).
- [35] I. B. Radović, Z. Siketić, M. Jakšić, and A. F. Gurbich, *J. Appl. Phys.* **104**, 074905 (2008).